Published, *International Journal of Fatigue*, Vol. 27/10-12, pp 1644-1652,
Fatigue Damage of Structural Materials V. December 2005

Early Detection and Monitoring of Fatigue in High Strength Steels with MWM-Arrays

V. Zilberstein [a,*], D. Grundy [a], V. Weiss [a], N. Goldfine [a], E. Abramovici [b], J. Newman [c], T. Yentzer [d]

[a] *JENTEK Sensors, Inc. 110-1 Clematis Avenue, Waltham, MA 02453, USA*
[b] *Bombardier Aerospace, Montreal, Quebec, Canada H3C 3G9*
[c] *Mississippi State University, Bagley College of Engineering, Mississippi, USA*
[d] *WR-ALC/ENFM, Robins AFB, GA 31098, USA*

Abstract

Fatigue monitoring of cyclically loaded shot peened high-strength steel components can be accomplished via magnetic permeability measurements during laboratory tests or in service. These measurements can be performed either continuously using permanently mounted Meandering Winding Magnetometer Arrays (MWM®-Arrays) or intermittently with scanning MWM-Arrays. The results obtained to date suggest that MWM-Array permeability measurements can provide early detection of fatigue damage in steels *before* conventional methods can detect any changes. This has been demonstrated to be particularly significant in the presence of high compressive stresses introduced by shot peening. One of the fatigue tests was suspended when accelerating changes in local permeability were detected. Examination of the fatigue specimen in a scanning electron microscope detected only a few relatively small cracks, e.g., 50 to 200 μm long at the surface. Fractography, however, revealed significantly longer cracks. For the same specimen, conventional eddy current and ultrasonic testing failed to provide any indications of cracks, and fluorescent liquid penetrant detected only an inconclusive spot indication. This paper provides a comparison of the permeability changes and fractography data with a fatigue crack growth curve based on a FASTRAN analysis accounting for residual stresses from shot peening. A comparison of the experimental data and crack growth analysis results suggested that MWM-Array magnetic permeability measurements may detect cracks in the compressive stress field when they are about 50 μm deep.

Keywords: Fatigue, High-strength steel, Fractography, Cracks in shot peened regions

1. Introduction

Fatigue critical areas, particularly in aircraft components, are often cold worked by shot peening, roller burnishing, or cold expansion to introduce compressive stresses. These compressive stresses significantly increase fatigue life, at least in the case of intermediate and high-cycle fatigue, typically well beyond the design life of the components. If, however, fatigue damage with ensuing fatigue crack initiation and growth does develop, it is important to detect it well before a crack may become critical. Timely detection and characterization of fatigue damage would allow prevention of a failure. Moreover, if fatigue damage is detected early enough, a corrective action, e.g., a minor rework, could become an option. Early damage detection is an integral part of Adaptive Damage Tolerance (ADT), an approach to component life management that requires improved observability of causative factors and material damage [1].

Until recently, early detection and characterization of fatigue damage was limited to laboratory methods, such as X-ray diffraction [2-5] and electron microscopy. Some of the following methods show promise for fatigue detection in metals and alloys: electrical conductivity [6] and magnetic permeability [7] measurement methods, ultrasonic wave distortion [8], laser diffraction [9], infrared thermography, acoustic microscopy, and positron annihilation [10].

Electrical conductivity and/or magnetic permeability measurements using the "Meandering Winding Magnetometer" (MWM) eddy current sensors and MWM-Arrays [11-15], provide a very practical and robust capability to measure and image magnetic and conducting properties of ferrous and nonferrous alloys on surfaces with complex geometries. A previous paper [7] described results of fatigue tests demonstrating the capability of permanently mounted and scanning MWM-Arrays to detect fatigue damage and tight cracks in shot peened high-strength steel components. The results of these tests as well as tests on aluminum [6] and nickel alloys demonstrated that permanently mounted MWM-Arrays can be used to stop fatigue tests, once cracks of specified sizes are detected in test specimens. Such specimens as discussed in Reference [16] would be valuable as standards for nondestructive inspection of bolt holes, e.g., in aircraft engine components. This paper provides a more detailed analysis of the previously presented results on fatigue monitoring of shot peened 4340 steel [7] and more recently performed fractography.

* Corresponding author. Tel.: 781-642-9666; Fax: 781-642-7525. Email address: jentek@shore.net

2. MWM-Arrays and Measurement Grids

The inductive MWM-Array sensor utilizes a meandering primary winding with numerous fully parallel secondary windings (sensing elements). Permanently mountable MWM-Arrays are particularly suited for continuous fatigue monitoring applications, e.g., for fatigue tests of specimens and components and for in-service monitoring at difficult-to-access locations. Scanning MWM-Arrays with multiple sensing elements provide the capability to generate images revealing, for example, localized damage and cracks. The scanning MWM-Arrays are particularly useful for aircraft and other structures where eddy current testing (ET) is already a widely accepted technique for inspection, while embedded MWM-Arrays provide a potential "alternate means of compliance" for these inspections.

In an MWM-Array, a drive winding, with linear drive segments is excited with a current at a prescribed frequency, typically from under 1 kHz up to 40 MHz, which provides a desired spatial distribution for the imposed magnetic field. The drive current produces a time varying magnetic field that induces eddy currents in conducting test materials that follow the drive winding pattern. Inductive sensing elements sense the absolute variations in the magnetic field due to the presence of the test material and local defects or geometric features that alter the flow of the induced eddy currents.

In the micro-fabricated MWM-Arrays, the windings are adhered to a conformable substrate, producing a very thin and flexible sensor. The MWM-Arrays used for this study are shown in Figure 1. Other example MWM-Arrays can be found in a number of papers [17-21].

The design of the drive winding produces a magnetic field in the material under test, such that it can be modeled with considerable accuracy. The software converts sensor impedance magnitude and phase response into material properties, such as electrical conductivity or magnetic permeability. A patented grid method is used to interpret data in real time using a database of responses [14, 15]. The database of responses is generated, prior to data acquisition, using a physical model of the sensor response to variations in material properties and layer thicknesses over the range of interest. Two-dimensional subsets of the database can be visualized as a measurement grid that relates two measured parameters (such as the magnitude and phase of the transimpedance between the MWM drive and sense windings) to two unknown parameters of interest, such as the magnetic permeability, electrical conductivity, and/or thickness of a material layer and the lift-off. Model based "grid measurement methods" provide automatic lift-off compensation and dramatically reduce calibration requirements. A portion of the grid used for monitoring of the 4340 steel fatigue tests discussed here is shown in Figure 2. Conventional iterative techniques for solving the inverse problem are relatively slow and are not guaranteed to converge to a physical solution. In contrast, the use of grid methods are guaranteed to converge as long as the data point falls within the grid and are relatively fast, making them well suited for the conversion of the image data into property estimates where tens of thousands of data points may need to be processed in real time.

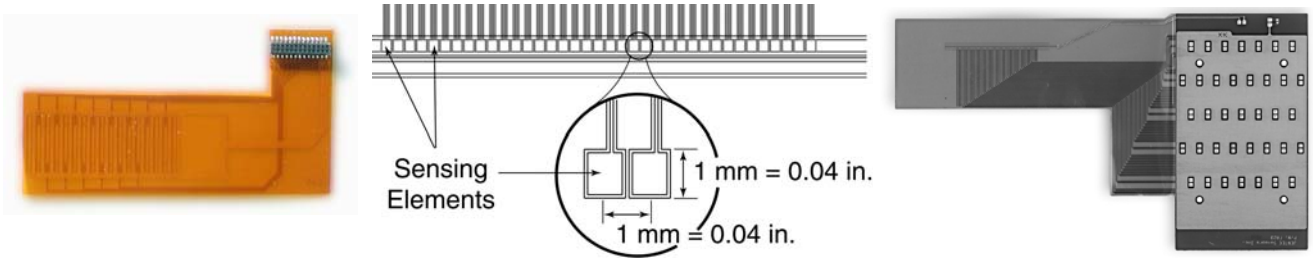

(a) (b) (c)

Figure 1. MWM-Arrays used in this study: (a) permanently mountable linear MWM-Array; (b), (c) scanning/ imaging MWM-Array schematic and photograph, respectively. The sensor in (a) was used for fatigue monitoring; the sensor in (b) and (c) was used to create the fatigue damage images after the tests.

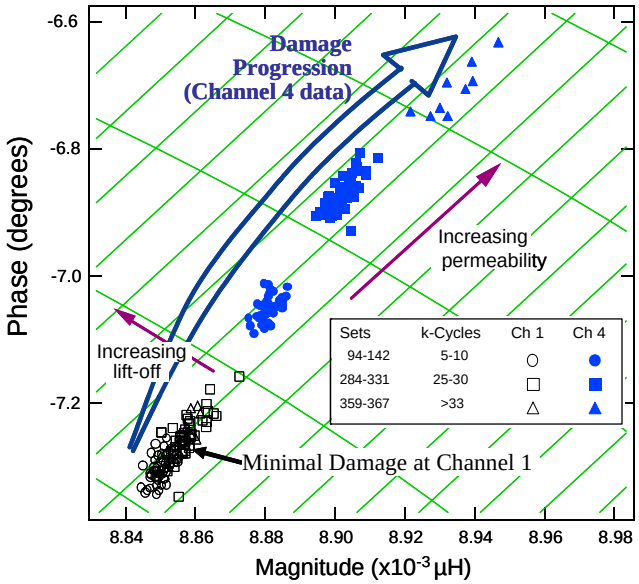

Figure 2. Detail of the measurement grid indicating response of four MWM-Array channels within selected ranges of load cycles. The fatigue damage progression in 4340 steel is reflected in the gradual increase of MWM-Array measured magnetic permeability.

3. Specimens and Test Procedure

The fatigue specimen design was selected based on a specific geometry requirement (presence of a cylindrical cavity) and stress distribution criteria. The key stress distribution criterion – higher stresses in the central portion of the cylindrical cavity – was verified by a finite-element analysis (FEA). In the FEA model, a 100 lb axial pulling force was applied. The resulting stress distribution is shown in Figure 3. Obviously, the cyclic loads in the tests were significantly higher so that the stresses used later in the fatigue crack growth analysis were scaled up.

The specimens were fabricated from 4340M steel heat treated to obtain high ultimate tensile strength (>200 ksi). The specimens were shot peened to generate high compressive residual stresses near the surface. Some of the specimens were also cadmium plated after shot peening to simulate typical high-strength components material constructs.

A linear MWM-Array with seven interleaved sensing elements located at 4-mm increments along the array length (see Fig. 1(a)) was mounted on the surface of the central cavity of the specimens. All seven sensing elements were located along the axis of the cavity. The outer sensing elements were located in the lower stress regions near the edges. During the fatigue tests, each of the seven sensing elements of the MWM-Array continuously monitored changes occurring in the material under the footprint of a sensing element. In the tests performed on a 9-ton Instron frame, the specimens were subjected to tension-tension cyclic loading at R = 0.1. The impedance measurement instrumentation provided the drive current to produce a spatially periodic magnetic field. The measurements were performed at frequencies of 39 kHz, 100 kHz, and 251 kHz. In this frequency range, the depth of sensor sensitivity for this steel is, perhaps, between 0.2 and 0.5 mm. However, the sensor can continue to monitor crack growth when a crack grows deeper than 0.5 mm due to crack length and crack opening increase at the surface.

The GridStation® software converted these data to local magnetic permeability so that results were obtained in terms of permeability measured at each individual sensing element within the MWM-Array. During fatigue testing, data is recorded continuously, without interrupting the test, at each channel using a seven-channel parallel architecture impedance instrument.

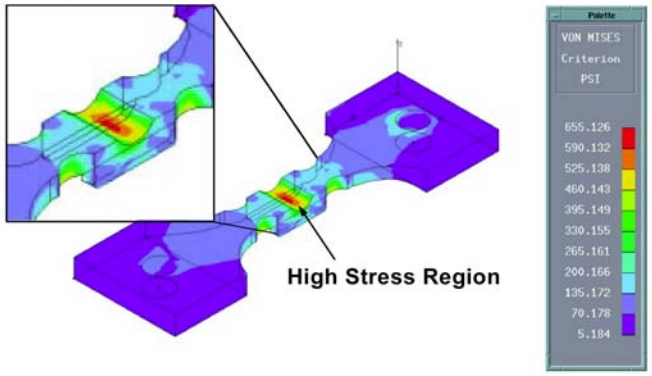

Figure 3. Distribution of stresses in the specimen FEA model. Note that the specimen was designed to have a nearly semicylindrical cavity in the center and the highest stress region in the middle of the central portion of the cavity.

4. Results

Both types of specimens i.e., (1) shot peened and (2) shot peened and cadmium plated, were subjected to fatigue testing using a constant amplitude loading. Results of the MWM permeability measurements made during a fatigue test of one of the shot peened specimens are presented in Figure 4. In this test, no significant permeability changes were detected within the first 7,000 cycles in any of the seven channels, i.e., over the entire 28-mm long section under the MWM-Array footprint. In the range between 7,000 and 31,000 cycles, all seven channels detected gradual permeability changes. However, these changes were significantly faster in the higher stress area compared to the areas near the edges where the FEA indicated substantially lower stresses. At about 31,000 cycles, two of the centrally located channels of the

MWM-Array showed a sharp increase of locally measured permeability, and the test was terminated at 33,500 cycles.

After the test, the central region of the specimen shown in Figure 4 (inset photo) was examined in a scanning electron microscope (SEM) and about twenty distinct cracks were reported. Most of them were fairly small, on the order of 50 μm long at the surface. The longest of the cracks detected in the SEM and shown in Figure 5 was about 200 μm long at the surface. This irregularly shaped crack appeared to consist of four nearly parallel "horizontal" cracks interconnected by nearly vertical cracks. This specimen was also examined by conventional eddy current, ultrasonic, fluorescent magnetic particle, and fluorescent liquid penetrant inspection. The fluorescent liquid penetrant inspection detected two small round indications, each less than 0.25 mm. The other nondestructive tests did not detect any indications. The cavity was then scanned with an imaging MWM-Array shown in Figures 1(b) and 1(c). During the scanning, the drive was oriented perpendicular to the axis of the coupon cavity, i.e., perpendicular to the anticipated predominant orientation of fatigue cracks. This orientation was the same as in fatigue test monitoring with a permanently mounted MWM-Array shown in Figures 1(a) and 4 (inset photo). Figure 6 (left) shows the permeability image obtained with the imaging MWM-Array. This image shows the distribution of fatigue damage in the high-stress area of the specimen and reveals two adjacent zones within the image with a higher permeability. The zone on the left contains two spots with the highest permeability.

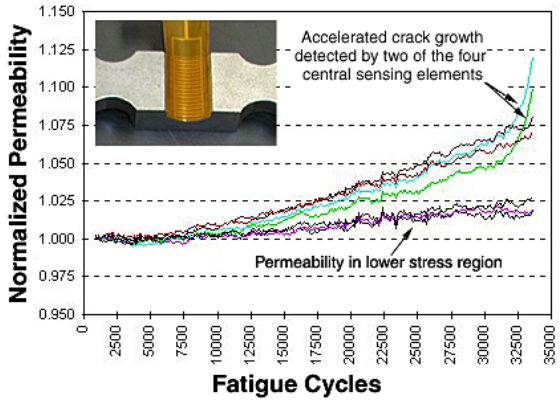

Figure 4. Normalized permeability vs. fatigue cycles as measured with an MWM-Array permanently mounted on a shot peened 4340 steel specimen. The initial permeability increase starting at about 7000-8000 cycles is attributed to early fatigue damage detection, possibly formation of microcracks within individual grains or at inclusions. A sharp increase detected by two of the four centrally located sensing elements above 31,000 cycles is caused by accelerated crack growth.

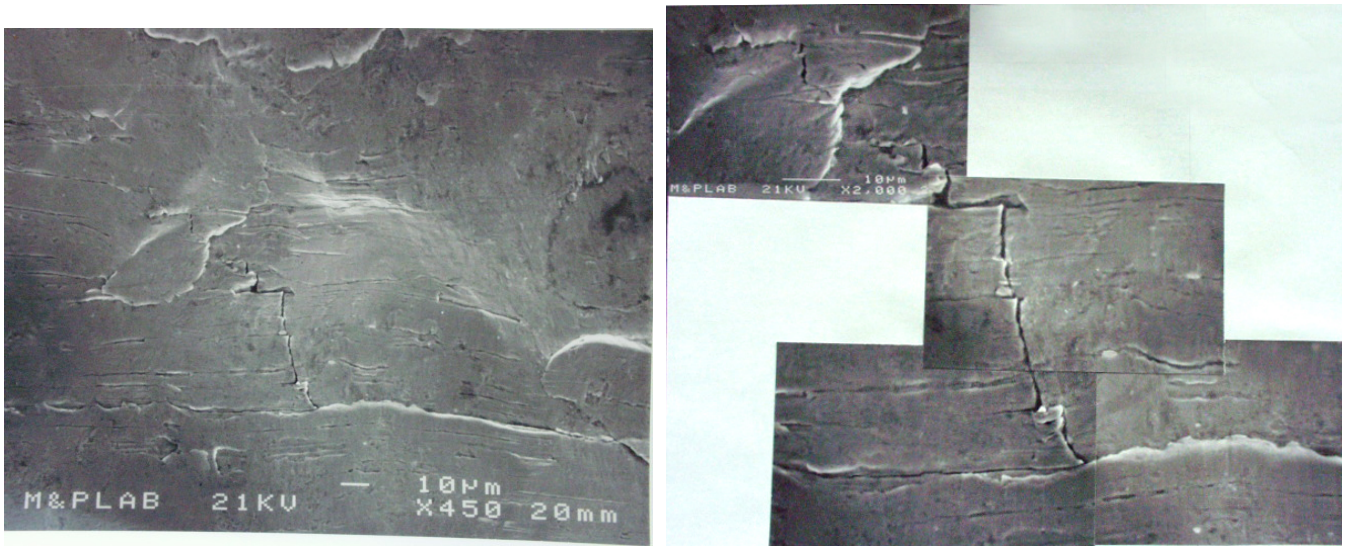

Figure 5. A major portion of the 200-μm long crack in the shot peened high-strength steel specimen. Note that this was the largest crack detected in this specimen (see the MWM data for this test in Figure 4).

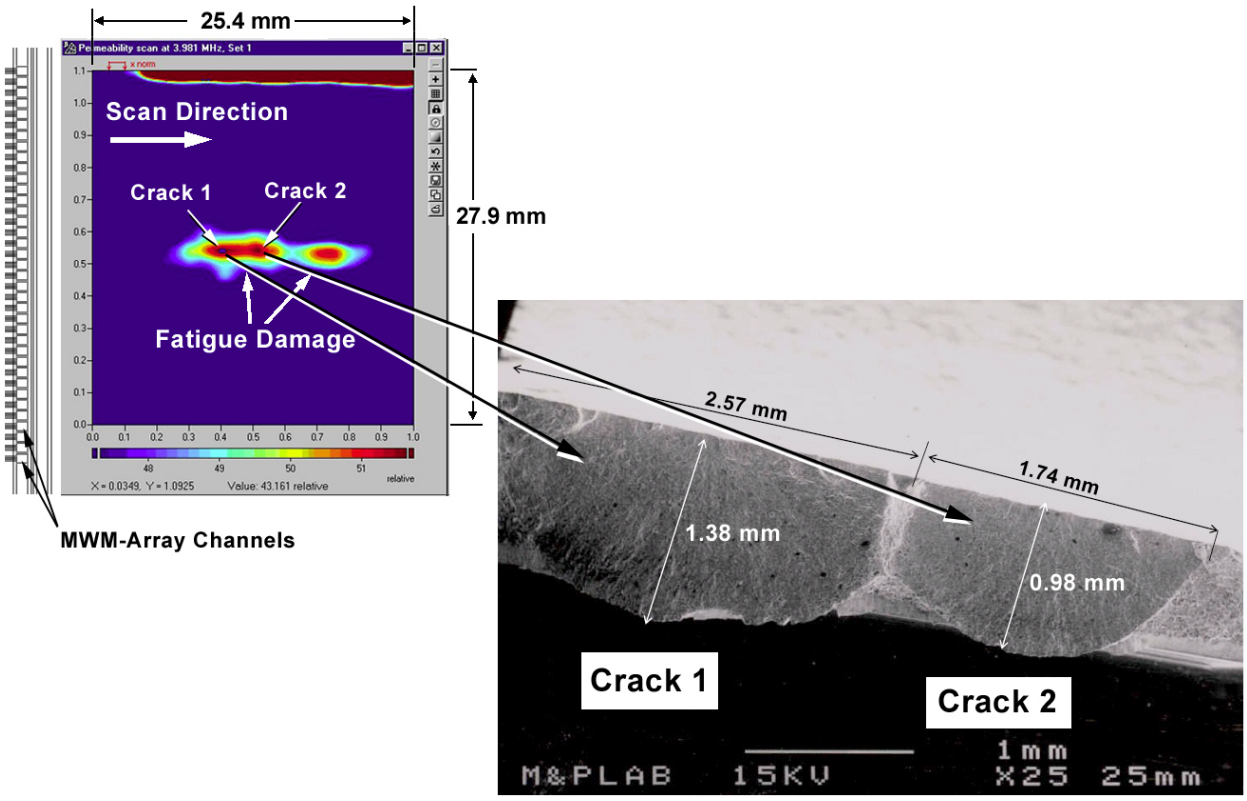

Figure 6. Fractography revealed two nearly coalesced cracks significantly larger than could be inferred from SEM observations.

5. Fractography

After the SEM of the central cavity region and MWM-Array imaging of the cavity were completed, the specimen was notched on the backside and, upon cooling in liquid nitrogen, was broken for a fractographic examination. Figure 6 shows fractography results revealing two nearly coalesced cracks. The larger crack is 1.38 mm deep and at least 2.57 mm long. The combined length of the two cracks is about 4.3 mm. Striation count was carried out at selected locations on both cracks. Estimated crack growth rates, da/dN, at the selected locations are tabulated in Table 1 below.

Table 1. Estimated Crack Growth Rates Based on Striation Spacing at Various Crack Depth

Crack 1		Crack 2	
a, mm	**da/dN, mm/cycle**	**a, mm**	**da/dN, mm/cycle**
		0.66	2.90E-04
0.84	4.35E-04	0.91	3.29E-04
0.95	2.80E-04	0.94	2.30E-04
1.38	2.88E-04	0.98	1.76E-04

The striation count suggested a reduced crack growth rate at some of the deeper locations. This can be attributed primarily to the changes in the applied stresses with depth as indicated by the FEA. Spatial variations in microstructure and residual stress redistribution could also contribute to crack growth rate variations. It appears that some of the MWM-Array sensing elements captured changes in the crack growth rate via changes in the slope of the measured magnetic permeability vs. cycles curves.

6. Analysis

The FEA indicated that the central region in the test specimen had the highest stresses (see Fig. 3) and a significant stress gradient through the thickness. An estimate of the normal stresses through the thickness and along the anticipated crack plane is shown by the upper dashed curve in Figure 7 (note that the distance from the surface, x, is plotted on a logarithmic scale). The maximum stress at the free surface (x = 0) was 1470 MPa. The assumed residual stresses due to shot peening are based on literature data [22] and are shown as the lowest dashed curve. This is an idealized curve as the actual distribution of compressive stresses at the surface is not uniform. The solid curve shows the maximum normal stress (σ_{max}), which was obtained by linear superposition of the applied normal stress due to remote loading and the residual-stress distribution. Under cyclic loading, the cyclic stress range will be unaffected by the residual-stress distribution, but the minimum stress at the shot-peened surface will go into compression over the first 0.15 mm and the minimum stress (σ_{min}) distribution is shown

by the lower dashed curve, as indicated. The solid symbol shows the assumed initial discontinuity size (30 μm radius), or the initial crack size for the FASTRAN analysis, of the 4340 steel. (This value was one of the largest inclusion particle sizes that had been observed in high-strength 4340 steel [23].)

Using the assumed normal stress distributions along the potential crack plane, the stress-intensity factor (K) at the maximum depth location for a surface crack emanating from the free surface (a/c = 1) is shown in Figure 8. The dashed and solid curves are the K values as a function of crack depth without and with residual stress, respectively. The approximate surface-crack solution was obtained by using a Green's function approach to calculate the stress-intensity factors for an edge crack [24] under the assumed stress distributions and then to multiply the edge-crack solution by 0.67. This will give approximate K values for a semi-circular surface crack under the assumed stress distributions. A table-lookup procedure was used in FASTRAN [25] to input the normalized stress-intensity factor as a function of normalized crack depth for the cases with and without residual stress. The applied stress ratio for the test specimen was R = 0.1. The no-residual-stress case had positive stress-intensity factors at minimum load (see lower dashed curve in Fig. 8). However, the shot-peened specimen developed negative minimum stress-intensity factors for crack depths less than about 0.5 mm. Because most of the fatigue life is consumed for crack less than 0.5 mm, the K_{min} value for the shot-peened specimen was assumed to be zero (crack surfaces were assumed to close at zero stress-intensity factor). This is a reasonable assumption for large surface cracks under nearly plane-strain conditions [26]. However, further study is needed because negative crack-opening stresses have been measured [27] and calculated [28] for small cracks less than 0.2 mm in length in aluminum alloys under negative stress ratios.

Figure 9 shows the effective stress-intensity factor against fatigue crack growth rate relationship (solid curve) that was used to make life calculations for the specimen with and without residual stress. The crack growth rate data were obtained from Swain et.al [23] for middle-crack tension specimens made of 4340 steel tested over a wide range of stress ratios. The crack-closure model [25] was used to correlate the crack-growth rate data using plane-strain constraint conditions (α = 2.5) for low rates and a transition to plane-stress conditions at higher rates. These results have been successfully used to predict "total" fatigue lives of 4340 specimens with a semi-circular edge notch and open-hole specimens subjected to constant-amplitude and helicopter spectrum loading [26].

A comparison of calculated and measured crack depth against cycles and crack depth against rate are shown in Figures 10 and 11, respectively. In the calculations, a single semi-circular surface crack was assumed to occur at the maximum normal stress location and propagate through the thickness. For the no residual stress case, R = 0.1 loading was used, but the shot-peened specimen was analyzed with R = 0 conditions to simulate the contacting crack surfaces under compressive stress-intensity factors. For large cracks, the calculated crack-opening stress levels are essentially the same for R = 0 and R < 0 for plane-strain conditions. The solid symbols in Figure 10 are crack depths measured on two surface cracks on the shot-peened specimen during the fractographic examination described in Section 5. Both cracks were nearly semi-circular and had partly coalesced. Figure 11 shows a comparison of the measured and calculated crack growth rates. The comparison between measured and calculated rates was quite good, but indicated that the measured rates were for cracks that had grown away from the influence of the residual-stress field. Future study is needed to measure rates at smaller crack lengths and to relate the assumed initial crack size to either metallurgical features in the material, machining marks, or to the shot-peened surface roughness. In addition, small cracks emanating from inclusions or surface marks in the steel may develop negative crack-opening stresses under compressive loading due to residual stresses.

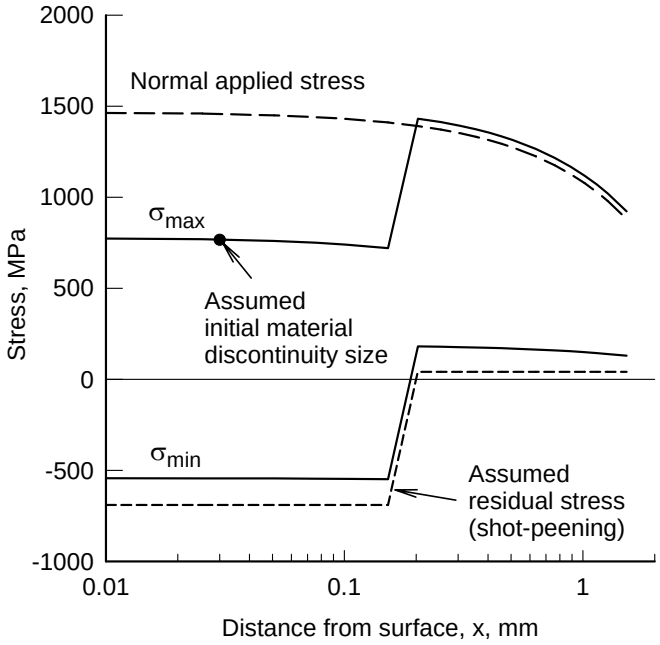

Figure 7. Stresses along crack plane with and without residual stresses.

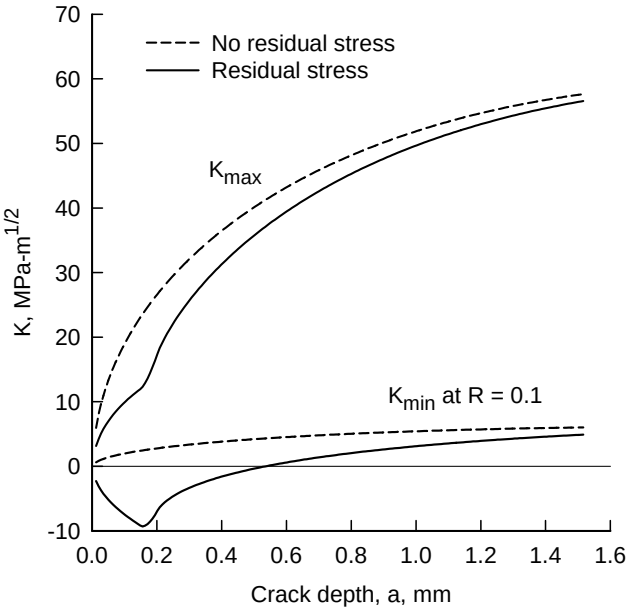

Figure 8. Stress-intensity factors for surface crack with and without residual stresses.

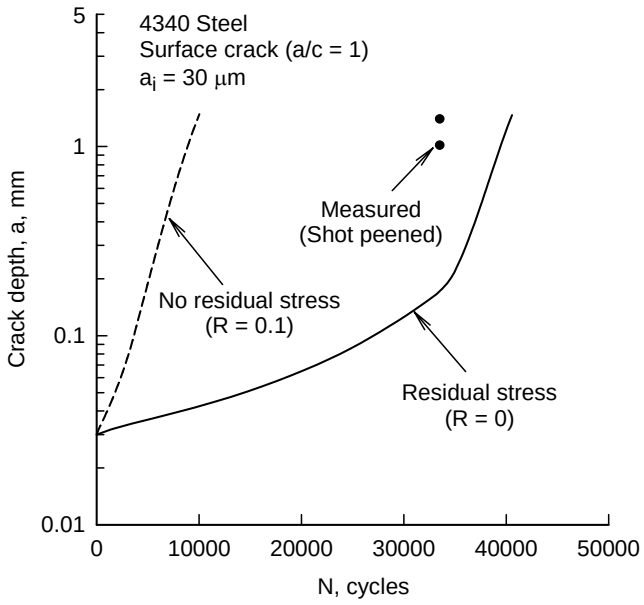

Figure 10. Calculated and measured crack depth against cycles for specimen with and without residual stresses.

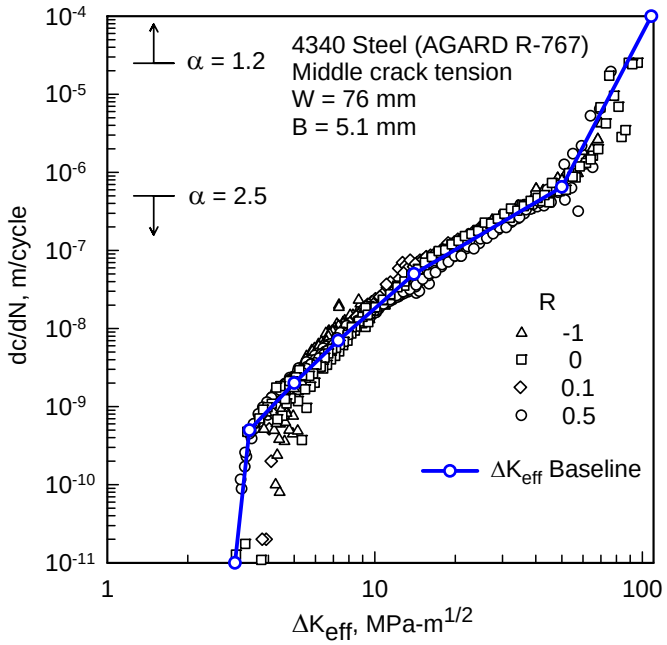

Figure 9. Effective stress-intensity factor against rate for high-strength 4340 steel.

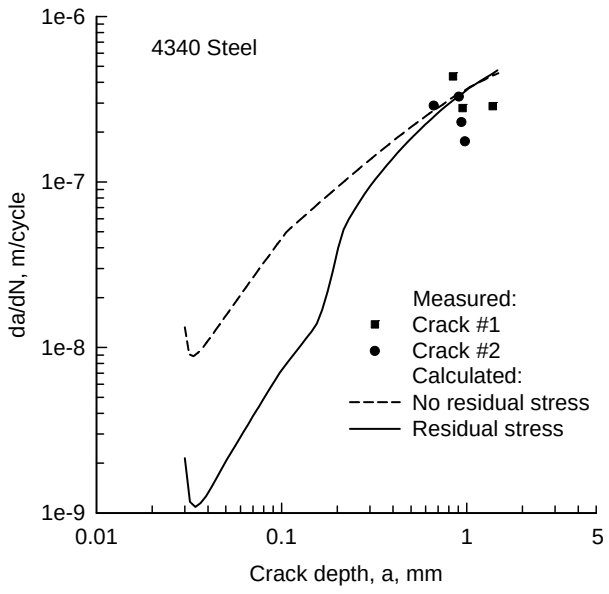

Figure 11. Calculated and measured rates for test specimen with and without residual stresses.

7. Discussion

Based on a comparison of the MWM-Array generated permeability image shown in Figures 4 and 6 (left), with the results of fractography, the two highest permeability spots within the left zone in the image correspond to the two adjacent cracks revealed by fractography. Many, if not all, of the other twenty short cracks observed during the SEM of the cavity, i.e., prior to breaking the specimen for fractography, were most likely a part of the two nearly coalesced cracks. The somewhat lower permeability "halo" that surrounds the MWM detected crack indications on the scanned image in the left zone as well as the entire right zone correspond, for the most part, to significant "precrack" fatigue damage. These zones may have contained microcracks, e.g., <3 μm, that could not be reliably detected in the SEM for these machined and shot peened surfaces, and, thus, could have been present but missed in the SEM. Data from the permanently mounted MWM-Array (see Figure 4) provides the history of fatigue damage accumulation. It detected an early onset of changes of the measured magnetic permeability and revealed a gradual magnetic permeability increase. It appears that this gradual magnetic permeability increase corresponds primarily to fatigue damage prior to formation of cracks or at least prior to formation of short cracks, e.g., cracks that are shorter than the grain size.

Figure 12 shows the FASTRAN generated fatigue crack growth curve and final crack depth values obtained from fractography (crack depth scale on the right) as well as the normalized MWM-Array measured permeability curves (left scale). This figure reveals that the permeability curves for the two central channels, indicating the accelerated permeability increase, reflect faster crack growth toward the end of the test. As an illustration of the MWM-Array capability, Figure 12 shows that at 17,000 cycles when two of the MWM-Array channels indicate a permeability increase as large as 2 percent, the estimated crack depth is about 50 μm. Note that a 2 percent change in permeability is an order of magnitude greater than the measurement noise. The MWM-Array can detect significantly smaller permeability changes that are likely to correspond to initial crack growth increments of just a few microns.

The results presented here suggest that permanently mounted MWM-Arrays can be used for fatigue studies of steel specimens or components to detect short cracks and monitor their growth. This capability can be used for early detecton of fatigue damage, i.e., early stage diagnostics (prior to formation of cracks detectable by traditional nondestructive methods) and for prognostics, i.e., assessment of how long a steel component can operate safely and when it should be reinspected. When required, MWM-Arrays can be mounted at critical locations on such components for inspections as frequently as required, even after every flight in the case of aircraft components. Scanning MWM-Arrays providing wide-area images of MWM measured permeabilities can also be used as frequently as practical. For some applications, the best solution will be a combination of MWM-Arrays permanently mounted at locations that can not be reached during inspections, without significant disassembly, and scanning MWM-Array for more accessible locations.

Furthermore, when local small cracks can be detected reliably in fatigue critical locations, life extension by local rework could provide a major cost reduction and life extension contribution. Following rework, MWM-Arrays could provide continuous or frequent periodic monitoring of repaired locations. This is relevant both for aging aircraft and design of new aircraft.

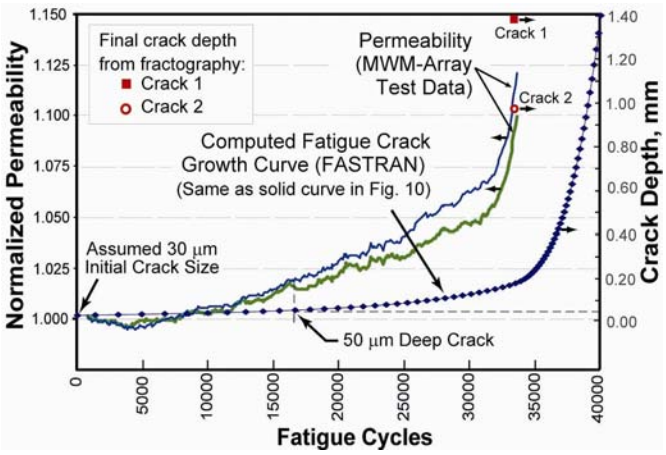

Figure 12. Fatigue crack growth curve (from FASTRAN analysis) superimposed on the MWM-Array measured magnetic permeability curves.

8. Concluding Remarks

MWM-Arrays provide the capability for continuous on-line monitoring of crack initiation and growth during fatigue tests of steel specimens and components. In low-alloy steels, permanently mounted MWM-Arrays can detect initial fatigue crack growth increments of just a few microns. In shot peened steel components, both permanently mounted and scanning MWM-Arrays can detect cracks that are difficult to detect by other nondestructive methods.

References

[1] Goldfine, N., and Zilberstein, V., Nondestructive Evaluation for CBM and PHM of Legacy and New Platforms, 57th MFPT Conference, Virginia Beach, VA, April 2003

[2] Regler F., Zeitschrift für Elektrochemie, v. 43, p. 546, 1937; Regler F. Verformung und Ermüdung Metallischer Werkstoffe, 1939.

[3] Taira S., Hayashi K. Proc. 9th Japanese Congress of Testing Materials, 1966.

[4] Kramer I.R. Metallurgical Transactions, v.5, p. 1735, 1974.

[5] Weiss V., Oshida Y. Fatigue Damage Characterization using X-Ray Diffraction Line Analysis. in Fatigue 84 1984; 1151.

[6] Zilberstein V., Schlicker D., Walrath K., Weiss V., Goldfine N. MWM eddy current sensors for monitoring of crack initiation and growth during fatigue tests and in service. International Journal of Fatigue 2001, Supplement: S477 – S485.

[7] Zilberstein, V., Walrath, K., Grundy, D., Schlicker, D., Goldfine, N., Abramovici, E., Yentzer, T., MWM Eddy-Current Arrays for Crack Initiation and Growth Monitoring, Published, *International Journal of Fatigue*, Volume 25, 2003, pp. 1147-1155.

[8] Cantrell J.H. Nonlinear Ultrasonic Characterization of Fatigue Microstructures. International Journal of Fatigue 2001; Supplement: S487 - S490.

[9] Gu Wenxuan, Lu Zhixian,Wang Anquiang Fatigue Damage Detection and Micromechanical Analysis of 30CrMnSi Materials Using Laser Diffraction. Chinese Journal of Applied Mechanics 1998, No1.

[10] Meyendorf N. Sathish S., Rosner H., Karpen W., Fassbender S., Sourkov A. NDE of Fatigue in Metals: Thermography, Acoustic Microscopy, and Positron Annihilation. 15th World Conference on Destructive Testing. Rome, Italy, October 2000.

[11] Melcher, J.R. Apparatus and methods for measuring permeability and conductivity in materials using multiple wavelength interrogations. US Patent Number 5,015,951, 14 May 1991.

[12] Goldfine, N.J. and Melcher, J.R. Magnetometer having periodic winding structure and material property estimator. U.S. Patent Number 5,453,689, 26 September 1995.

[13] Goldfine, N.J. and Melcher, J.R. Apparatus and methods for obtaining increased sensitivity, selectivity and dynamic range in property measurement using magnetometers. U.S. Patent 5,629,621, 2 June 1995.

[14] Goldfine, N.J. Magnetometers for improved materials characterization in aerospace applications. Materials Evaluation 1993; March: 396-405.

[15] Goldfine, N.J., Clark, D.C., Walrath, K.E., Weiss, V., Chepolis, W.M. Method of detecting widespread fatigue and cracks in a metal structure. US Patent Number 6,420,867, 16 July 2002.

[16] Goldfine N., Zilberstein V., Washabaugh A., Weiss V., Grundy D., The Use of Fatigue Monitoring MWM-Arrays in Production of NDI Standards with Real Fatigue Cracks for Reliability Studies, 16th World Conference on Nondestructive Testing, Montreal, Canada; August-September, 2004

[17] Goldfine, N.J., Zilberstein, V., Schlicker, D., Sheiretov, Y., Walrath, K., Washabaugh, A., Van Otterloo, D. Surface mounted periodic field eddy current sensors for structural health monitoring. Smart Structures and Materials, NDE for Health Monitoring and Diagnosis, ed. by T. Kundu, SPIE Conference Proceedings, Newport Beach, CA, 4335, 2001 pp. 20-34.

[18] Goldfine, N., Schlicker, D., Sheiretov, Y., Washabaugh, A., Zilberstein, V., Grundy, D. Surface mounted and scanning periodic field eddy-current sensors for structural health monitoring. IEEE Aerospace Conference: Prognostics & Health Management for Aging Aircraft, Big Sky, Montana, March 2002.

[19] Goldfine, N.J., Zilberstein, V., Cargill, J.S., Schlicker, D., Shay, I., Washabaugh, A., Tsukernik, V., Grundy, D., Windoloski, M. MWM-Array eddy current sensors for detection of cracks in regions with fretting damage. ASNT Materials Evaluation, 2002; July: 60, 870-877.

[20] Goldfine, N.J., Grundy, D., Zilberstein, V., Kinchen, D. Friction stir weld inspection through conductivity imaging using shaped field MWM-Arrays. International Conference on Trends in Welding Research, ASM International, Calloway Gardens, GA, 2002.

[21] Zilberstein, V., Fisher, M., Grundy, D., Schlicker, D., Tsukernik, V., Vengrinovich, V., Goldfine, N. Residual and applied stress estimation from directional magnetic permeability measurements with MWM sensors. Journal of Pressure Vessel Technology, 2002; August: 24, 375-381.

[22] Wohlfahrt, H. Shot peening and residual stresses. Residual Stress and Relaxation, The 28th Sagamore Army Materials Research Proceedings, ed. E Kula and V. Weiss, 1982, pp. 71-92.

[23] Swain, M., Everett, R., Newman, J. and Phillips, E. The growth of short crack in 4340 steel and aluminum-lithium 2090. AGARD Report No. 767, P. Edwards and J. Newman (eds), 1990; 7.1-7.30.

[24] Tada, H., Paris, P. and Irwin, G., The stress analysis of cracks handbook. The American Society of Mechanical Engineers, New York, NY, 2000.

[25] Newman, J. FASTRAN II - fatigue crack growth structural analysis program, NASA TM-104159, Feb. 1992.

[26] Newman, J. The merging of fatigue and fracture mechanics concepts - a historical perspective. Fatigue and Fracture Mechanics - 28th Volume, ASTM STP-1321, 1997; pp3-51.

[27] Lee, J. and Sharpe, W. Short fatigue cracks in notched aluminum specimens. Small Fatigue Cracks, R. Ritchie and J. Lankford (eds.), 1986; pp323-339.

[28] Newman, J., Swain, M. and Phillips, E. An assessment of the small-crack effect for 2024-T3 aluminum alloy. Small Fatigue Cracks, R. Ritchie and J. Lankford (eds.), 1986; pp 427-452.